



# CHALMERS

## Chalmers Publication Library

### Controlling drug delivery kinetics from mesoporous titania thin films by pore size and surface energy

This document has been downloaded from Chalmers Publication Library (CPL). It is the author's version of a work that was accepted for publication in:

**International Journal of Nanomedicine (ISSN: 1178-2013)**

#### Citation for the published paper:

Karlsson, J. ; Atefyekta, S. ; Andersson, M. (2015) "Controlling drug delivery kinetics from mesoporous titania thin films by pore size and surface energy". International Journal of Nanomedicine, vol. 10 pp. 4425-4436.

<http://dx.doi.org/10.2147/ijn.s83005>

Downloaded from: <http://publications.lib.chalmers.se/publication/220085>

Notice: Changes introduced as a result of publishing processes such as copy-editing and formatting may not be reflected in this document. For a definitive version of this work, please refer to the published source. Please note that access to the published version might require a subscription.

Chalmers Publication Library (CPL) offers the possibility of retrieving research publications produced at Chalmers University of Technology. It covers all types of publications: articles, dissertations, licentiate theses, masters theses, conference papers, reports etc. Since 2006 it is the official tool for Chalmers official publication statistics. To ensure that Chalmers research results are disseminated as widely as possible, an Open Access Policy has been adopted. The CPL service is administrated and maintained by Chalmers Library.

(article starts on next page)

 Open Access Full Text Article

ORIGINAL RESEARCH

# Controlling drug delivery kinetics from mesoporous titania thin films by pore size and surface energy

**Johan Karlsson****Saba Atefyekta****Martin Andersson**Department of Chemical  
and Biological Engineering, Chalmers  
University of Technology, Gothenburg,  
Sweden

**Abstract:** The osseointegration capacity of bone-anchoring implants can be improved by the use of drugs that are administrated by an inbuilt drug delivery system. However, to attain superior control of drug delivery and to have the ability to administer drugs of varying size, including proteins, further material development of drug carriers is needed. Mesoporous materials have shown great potential in drug delivery applications to provide and maintain a drug concentration within the therapeutic window for the desired period of time. Moreover, drug delivery from coatings consisting of mesoporous titania has shown to be promising to improve healing of bone-anchoring implants. Here we report on how the delivery of an osteoporosis drug, alendronate, can be controlled by altering pore size and surface energy of mesoporous titania thin films. The pore size was varied from 3.4 nm to 7.2 nm by the use of different structure-directing templates and addition of a swelling agent. The surface energy was also altered by grafting dimethylsilane to the pore walls. The drug uptake and release profiles were monitored *in situ* using quartz crystal microbalance with dissipation (QCM-D) and it was shown that both pore size and surface energy had a profound effect on both the adsorption and release kinetics of alendronate. The QCM-D data provided evidence that the drug delivery from mesoporous titania films is controlled by a binding–diffusion mechanism. The yielded knowledge of release kinetics is crucial in order to improve the *in vivo* tissue response associated to therapeutic treatments.

**Keywords:** mesoporous titania, controlled drug delivery, release kinetics, alendronate, QCM-D

## Introduction

When treating patients with drugs, it is essential to control the release rate of the active pharmaceutical ingredient to provide the optimized therapeutic drug concentration over a desired period of time. A recent strategy to improve osseointegration of bone-anchoring implants is to design devices having an inbuilt drug delivery functionality to obtain a specific and improved tissue response enhancing the ability of bone regeneration.<sup>1,2</sup> Alendronate (ALN) is an osteoporosis drug belonging to the group of bisphosphonates that is known to promote bone formation by its action of inhibiting osteoclastic activity.<sup>3–6</sup> Today, ALN is frequently used in clinics, often through oral administration. However, such systemic delivery of bisphosphonates has been associated with complications during oral surgical treatments, including osteonecrosis of the jaw.<sup>7</sup> Since ALN also has shown to improve the osseointegration of implants, eg, dental implants, it is important to find alternative administrative routes. A controlled local delivery system might bring an efficient therapeutic treatment, since it would administrate the drug directly at the targeted cells for a

---

Correspondence: Johan Karlsson  
Department of Chemistry and Chemical  
Engineering, Chalmers University of  
Technology, Kemivägen 10, 412 96  
Gothenburg, Sweden  
Tel +46 31 772 3006  
Fax +46 31 160 062  
Email johan.karlsson@chalmers.se

prolonged time period, and thus reduce the risk of systemic side effects. One strategy to achieve such local delivery from implants would be to apply a mesoporous coating. Mesoporous materials have been highlighted within nanomedicine as a promising drug delivery system, since they possess unique features, such as high specific surface area, and tunable pore-size, -volume, and -symmetry.<sup>8–14</sup> They are usually formed utilizing structure-directing agents functioning as template molecules.<sup>15</sup> The well-defined pore properties that are obtained with this synthesis procedure allow for a drug release in a highly reproducible and predictable manner. The most established template-based method for the formation of mesoporous thin films is the evaporation-induced self-assembly (EISA), in which surfactant self-assembly in the presence of inorganic precursor is utilized.<sup>16–18</sup> The most commonly used inorganic framework for ordered mesoporous materials is silica. However, for bone-anchoring implants, titania has been demonstrated suitable to use, since it is biocompatible and also a bioactive material providing direct surface formation of apatite in vivo, which subsequently enables bone bonding.<sup>19,20</sup> It is crucial for implants to ensure bone bonding in order to achieve proper interlocking of the implant.<sup>21–24</sup> In a previous study, we experimentally demonstrated ex vivo that Ca ions are directly attached to a mesoporous titanium oxide surface.<sup>25</sup> The ability of mesoporous titania to form a chemical bond with apatite in combination with functioning as a local drug delivery system would give unique properties when used as an implant coating. Moreover, in a previous study, it was demonstrated that mesoporous titania has good biomechanical stability toward the shearing forces that arises during implantation procedure, which also strengthen its usefulness as an implant coating.<sup>26</sup> It has also been shown in vivo that an enhanced osseointegration can be achieved using mesoporous titania with a pore size of 6 nm as the drug delivery system<sup>27–29</sup> and that it provides a sustained drug delivery in vivo.<sup>30</sup>

Quartz crystal microbalance with dissipation (QCM-D) is a suitable technique for in situ monitoring of adsorption- and desorption-kinetics of molecules to/from surfaces, which provides a high mass sensitivity.<sup>31</sup> Such information of kinetics is essential to further understand the adsorption and release mechanisms that take place at the different regimes. In this study, we have used QCM-D to examine how the release rate of ALN can be controlled by altering pore size and surface energy of mesoporous titania thin films. The pore size was varied using different structure-directing agents and by addition of a swelling agent. Furthermore,

surface functionalization using silane chemistry was used to change the surface energy of the pore walls. The physical and chemical properties of the different formed mesoporous films were characterized by scanning electron microscopy (SEM), transmission electron microscopy (TEM), synchrotron small angle X-ray scattering (SAXS), contact angle (CA) measurements, QCM-D, and X-ray photoelectron spectroscopy (XPS). In situ monitoring of the drug adsorption and release kinetics was carried out using QCM-D, with emphasis on exploring the release kinetics as a function of pore size and surface energy of the mesoporous titania. The release kinetic mechanisms when using mesoporous materials as drug carriers were evaluated, which is something that was not well understood prior to this study.<sup>10</sup>

## Materials and methods

### Formation of mesoporous titania thin films and surface modification

Mesoporous titania thin films were formed using the EISA method.<sup>16,17</sup> In the synthesis, different structure-directing agents were used in order to predetermine the pore size of the titania matrix. BRIJ® S10 (Sigma-Aldrich, Steinheim, Germany) (polyoxyethylene (10) stearyl ether),<sup>32</sup> cetyltrimethylammonium bromide (CTAB, Sigma-Aldrich) ( $\text{CH}_3(\text{CH}_2)_{15}\text{N}^+(\text{CH}_3)_3\text{Br}^-$ ),<sup>33</sup> and Pluronic® P123 (P123, Sigma-Aldrich) (a triblock copolymer of  $\text{EO}_{20}\text{PO}_{70}\text{EO}_{20}$ )<sup>34,35</sup> were all used separately. Moreover, P123 was combined with poly(propylene glycol) (PPG,  $M_n \sim 4,000$ , Sigma-Aldrich) and used as a swelling agent to increase the pore size even further.<sup>36,37</sup> Two different mass ratios between PPG and P123 were used: 0.5 (PPG – 0.5) and 1 (PPG – 1). In all syntheses, the structure-directing agents, and, if used, the swelling agent (PPG) were dissolved in concentrated ethanol. In a separate vial, the inorganic precursor titanium(IV) ethoxide (TEOT, Sigma-Aldrich) was dissolved in concentrated (37%) hydrochloric acid (HCl, Sigma-Aldrich) with vigorous stirring for 3 hours. Then, the two solutions were mixed together with stirring for 1 hour to obtain a homogenous and clear mixture. All the specific amounts used in the different syntheses are presented in Table 1. The ratio between the template and the inorganic precursor was chosen to form mesoporous titania thin films with a cubic structure. The different mesoporous titania thin films were formed onto Ti discs, glass slides, and Ti QCM-D sensors. The film-formation method employed was spin-coating, where 70  $\mu\text{L}$  of the final solution was added prior to applying the processing condition using a rotational speed of 7,000 rpm (60 seconds). The prepared films were aged at room temperature overnight to obtain complete

**Table I** The different chemicals and their amounts that were used in the syntheses

| Sample   | Template (g) | Swelling agent (g) | TEOT (g) | HCl (g) | Ethanol (g) |
|----------|--------------|--------------------|----------|---------|-------------|
| CTAB     | 0.74         | –                  | 2.1      | 1.65    | 12          |
| BRIJ S10 | 0.52         | –                  | 2.1      | 0.7     | 12          |
| P123     | 0.5          | –                  | 2.1      | 1.6     | 8.5         |
| PPG-0.5  | 0.65         | 0.32               | 2.1      | 1.53    | 6           |
| PPG-1    | 0.65         | 0.65               | 2.1      | 1.53    | 6           |
| NP       | –            | –                  | 2.1      | 1.6     | 8.5         |

**Notes:** The samples are named according to the used template or ratio of the swelling agent PPG. – Specified chemical was not used in the synthesis of the specified sample group.

**Abbreviations:** TEOT, titanium(IV) ethoxide; CTAB, cetyltrimethylammonium bromide; PPG, poly(propylene glycol); NP, nonporous.

self-assembly. An exception was made for the syntheses, including PPG, where the storage overnight was done in a refrigerator at 4°C. The final step was calcination, in which the template was removed to obtain the porous solid films. The calcination procedure involved heating the samples at a rate of 1°C/min until it reached 350°C, at which time it was kept for 4 hours and then slowly cooled down to room temperature. Nonporous (NP) samples were prepared using the same synthesis route; however, without the addition of structure-directing agent.

In order to adjust the surface energy, surface functionalization using silane chemistry was performed to obtain a methylated surface. More specifically, dichlorodimethylsilane (DCDMS, Sigma-Aldrich) was dissolved in methanol at a concentration of 5 wt%. The samples to be surface-modified were first pretreated in a water (deionized) bath for 45 minutes at 25°C to increase the amount of hydroxyl groups on the surface.<sup>38,39</sup> The samples were then immersed in the DCDMS solution for 15 minutes. After that, they were rinsed with chloroform, followed by again being immersed into the DCDMS solution for 45 minutes. Nitrogen gas was thereafter used to dry the samples.

## Scanning electron microscopy

SEM was performed to provide structural information, such as pore width, pore direction, and film thickness for the different mesoporous titania films. The instrument used was a Leo Ultra55 (Carl Zeiss Meditec AG, Oberkochen, Germany) equipped with a field emission electron gun, operated at an accelerating voltage of 5 kV. Images were acquired using an in-lens secondary electron detector. The mesoporous titania thin films were deposited onto Ti discs for the SEM analysis, and due to proper conductivity, no sputter coating was needed. Furthermore, SEM was also used to determine the film thickness of the different mesoporous films. In this analysis, a special sample holder was used into which cross-sections of mesoporous-coated glass slides could be mounted. Mesoporous-coated glass slides, which were sputter coated

with a few-nanometer-thick gold layer to avoid charging of the specimens, were used for the cross-sectional analysis.

## Transmission electron microscopy

The mesoporous titania films were characterized using TEM to examine the pore width. TEM micrographs were captured using a JEOL 1200-EX II microscope (JEOL Ltd., Tokyo, Japan) operated at an accelerating voltage of 120 kV. Microscopy specimens were prepared by first scraping off the mesoporous titania coatings deposited onto glass slides. The collected powder was ground and dispersed in ethanol, followed by sonication for 5 minutes to achieve a proper suspension. The suspension was added (~2 µL) onto TEM grids (carbon 300 mesh, Capilor AB, Helsingborg, Sweden) and dried at room temperature prior to the TEM analysis.

## Synchrotron small angle X-ray scattering

SAXS was utilized to obtain structural information, including if any long-range order existed in the mesoporous titania films. The measurements were performed at the MAX IV Laboratory (Lund, Sweden) on beamline I911-4. Data were collected with a *q*-range ( $q = 4\pi \sin\theta/\lambda$ ) of 0.1–3.0 nm<sup>-1</sup>. A beam size of 1.2×1.2 Å was used, with a fixed wavelength of 0.91 Å. Prior to analysis, the specimens were prepared by collection and grinding of scraped-off powder from coated glass slides.

## X-ray photoelectron spectroscopy

XPS was performed to examine the surface chemistry of the mesoporous titania thin films, in order to verify that the pore size was tuned without changing the surface chemistry. The instrument used was a Quantum 2000 scanning XPS microscope (Physical Electronics, Chanhassen, MN, USA) equipped with a monochromatic Al  $K_{\alpha}$  (1,486.6 eV) X-ray source with beam size 100 µm and a takeoff angle of 45°. On characterization, the analyzed point diameter was 100 µm, and the depth of the analysis was 4–5 nm. The coatings to be analyzed were deposited onto Ti discs.

## Contact angle

Static CA was utilized to determine the surface free energy of the mesoporous titania thin films, both with and without surface modification. CA measurements were performed on glass slides, coated with the different mesoporous titania thin films using an Attension Theta optical tensiometer (KSV, Helsinki, Finland), where water (Milli-Q,  $\gamma=72.8 \text{ mN/m}$ ) was used as liquid. Triplicates ( $n=3$ ) of each sample group were analyzed, and the results were presented as an average value.

## Pore volume measurement

The accessible pore volume for water in the mesoporous coatings was measured using QCM-D, utilizing a Q-Sense E4 instrument (Q-Sense, Gothenburg, Sweden). The different mesoporous titania thin films were deposited onto QCM-D titanium sensors (QSX 310, Q-Sense) according to the spin-coating procedure described under “Formation of mesoporous titania thin films and surface modification”. A flow of pure  $\text{H}_2\text{O}$  (Milli-Q) was first added until a stable baseline was achieved. Thereafter, the flow of  $\text{H}_2\text{O}$  was changed to  $\text{D}_2\text{O}$  and the frequency ( $\Delta f$ ) and dissipation ( $\Delta D$ ) shifts were recorded as a function of time.  $\Delta f$  corresponds to the density difference between  $\text{D}_2\text{O}$  that has accessed the pores and  $\text{H}_2\text{O}$  that previously occupied the pore volume, and what this corresponds to in mass was calculated using the Sauerbrey equation.<sup>40</sup> As a reference, the experiment was also carried out on the NP counterpart. From these data, together with the film thickness data measured by SEM, the specific pore volume of the mesoporous films was calculated.

## In situ drug adsorption and release

QCM-D measurements were carried out to evaluate adsorption and release kinetics of ALN (alendronate monosodium trihydrate, LKT Laboratories, St Paul, MN, USA) in situ. Due to the high sensitivity of the technique, even adsorption and desorption of small-molecular drugs can be monitored without the use of probes. Prior to experiments, QCM-D titanium sensors (QSX 310, Q-Sense) were coated with mesoporous titania thin films. The experiments were performed with a Q-Sense E4 instrument (Q-Sense). The QCM-D measurements were initiated by flowing pure Milli-Q  $\text{H}_2\text{O}$  (50 mL/min) until a stable baseline was reached. Then, ALN dissolved in water (0.8 mg/mL) was added with a flow rate of 50 mL/min to monitor the adsorption of ALN to the surfaces. This was continued until complete loading was achieved. Thereafter, the surfaces were rinsed using Milli-Q  $\text{H}_2\text{O}$  (50 mL/min) to follow the drug-release behavior. The drug loading and release were monitored as changes in frequency ( $\Delta f$ , Hz) and dissipation ( $\Delta D$ ).  $\Delta f$  was converted

to mass ( $\text{ng}/\text{cm}^2$ ) of adsorbed active substance using the Sauerbrey equation.<sup>40</sup>

## Results

### Material characterization

Three different structure-directing agents, CTAB, BRIJ S10, and P123, were used in the synthesis of mesoporous titania thin films to vary the pore size. In addition, PPG was used as a swelling agent to increase the pore size even further. SEM was used to visualize the mesopores of the different coatings, as shown in Figure 1. The collected micrographs demonstrated that all the different surfaces possessed a high degree of porosity with a narrow pore-size distribution. In addition, the ratios used between the template and the inorganic precursor were chosen to form mesoporous titania thin films with a cubic symmetry to ensure accessible pores toward the surrounding, which is a prerequisite to use them as coatings for drug delivery purposes. The presence of pores directed out from the surface was observed in the SEM images.

In addition, TEM was utilized to visualize the pores of the different mesoporous titania films. TEM micrographs of the samples prepared with different structure-directing agents and the addition of a swelling agent are presented in Figure 2. The TEM images supported the findings from the SEM characterization that the materials possess a high degree of porosity with a narrow pore-size distribution within all the sample groups.

Pore-size measurements were carried out using both the SEM and TEM images, and the result of the average pore size for the different groups is presented in Table 2. The different structure-directing agents altered the average pore size from 3.4 nm up to 6.0 nm. When the synthesis with P123 was carried out with PPG as the swelling-agent, an average pore width as large as 7.2 nm was obtained.

SEM was also used to determine the film thickness of the mesoporous titania coatings. Cross-sections of mesoporous-coated glass slides were prepared for all the different samples, and the film thickness was measured in the acquired SEM images. All coatings prepared without the addition of swelling-agents (CTAB, BRIJ S10, and P123) had a thickness of about 200–300 nm; whereas, the thickness for the coatings prepared with swelling-agents (PPG-0.5 and PPG-1) was about 700–800 nm. In Figure 3, SEM images of a mesoporous coating prepared with BRIJ S10 and a sample of PPG-0.5 are shown.

The obtained synchrotron SAXS data are presented in Figure 4. As can be seen, peaks were observed for all mesoporous samples, which demonstrated that a long-range order in the porous structures existed. It was not possible to

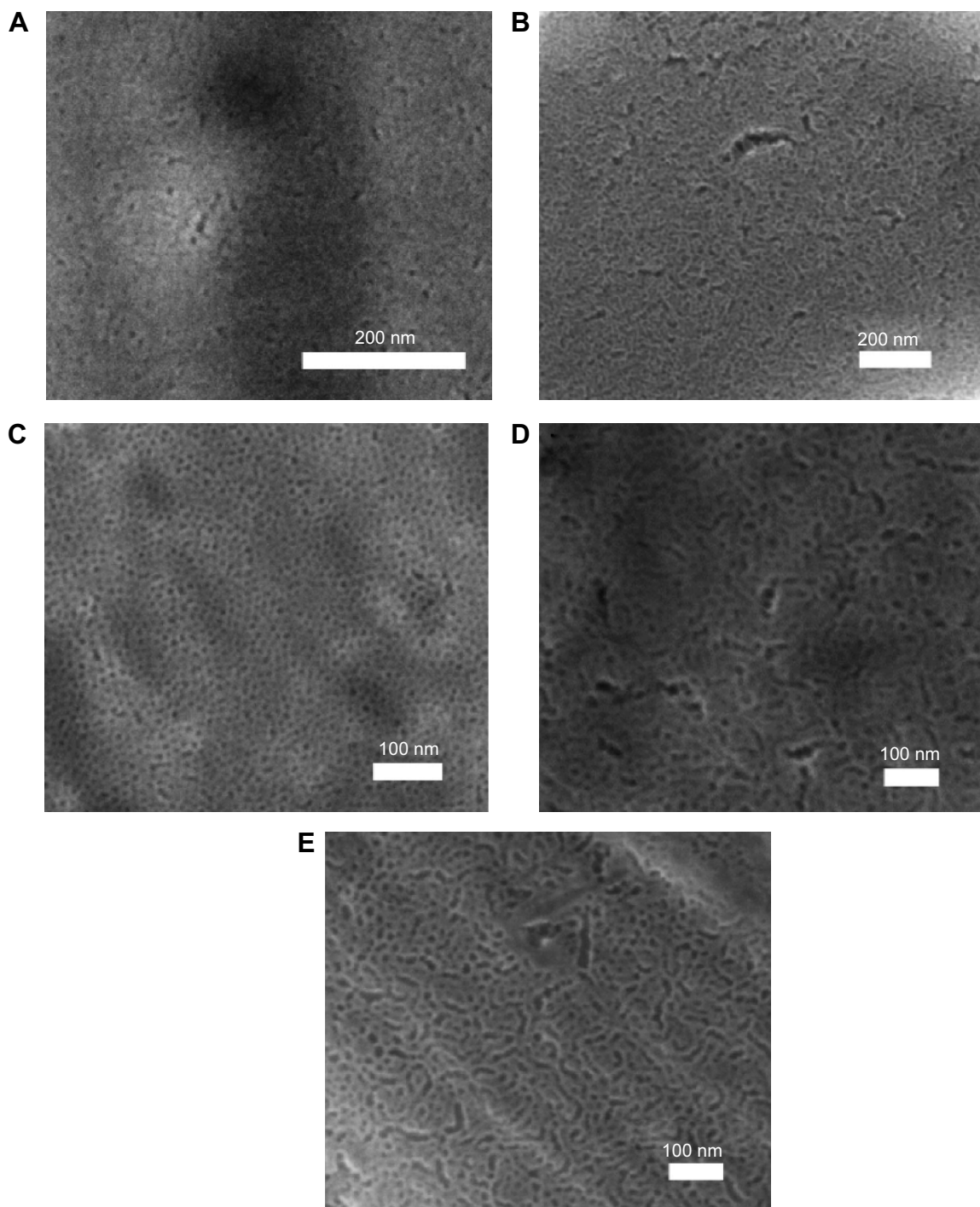


**Figure 1** SEM micrographs of mesoporous titania thin films.

**Notes:** SEM micrographs of mesoporous titania thin films prepared with the following structure-directing agents: **(A)** CTAB, **(B)** BRIJ S10, **(C)** PI23, **(D)** PI23 and PPG as swelling agents with a ratio of 1:0.5 (PPG-0.5), and **(E)** PI23 and PPG as a swelling agent with a ratio of 1:1 (PPG-1).

**Abbreviations:** CTAB, cetyltrimethylammonium bromide; PPG, poly(propylene glycol); SEM, scanning electron microscopy.

determine the pore symmetry from the SAXS data, since they only demonstrated one peak. The peak position was shifted toward lower  $q$ -values as the pore width increased. For the NP titania, no peaks were found.

XPS analysis was performed to verify that the pore size of the mesoporous titania thin films was tuned without

changing the surface chemistry. The obtained XPS data for the different mesoporous titania thin films possessing different pore sizes are presented in Table 3. No significant differences could be observed between the different surfaces; hence, the nanoporosity was tuned without altering the surface chemistry.

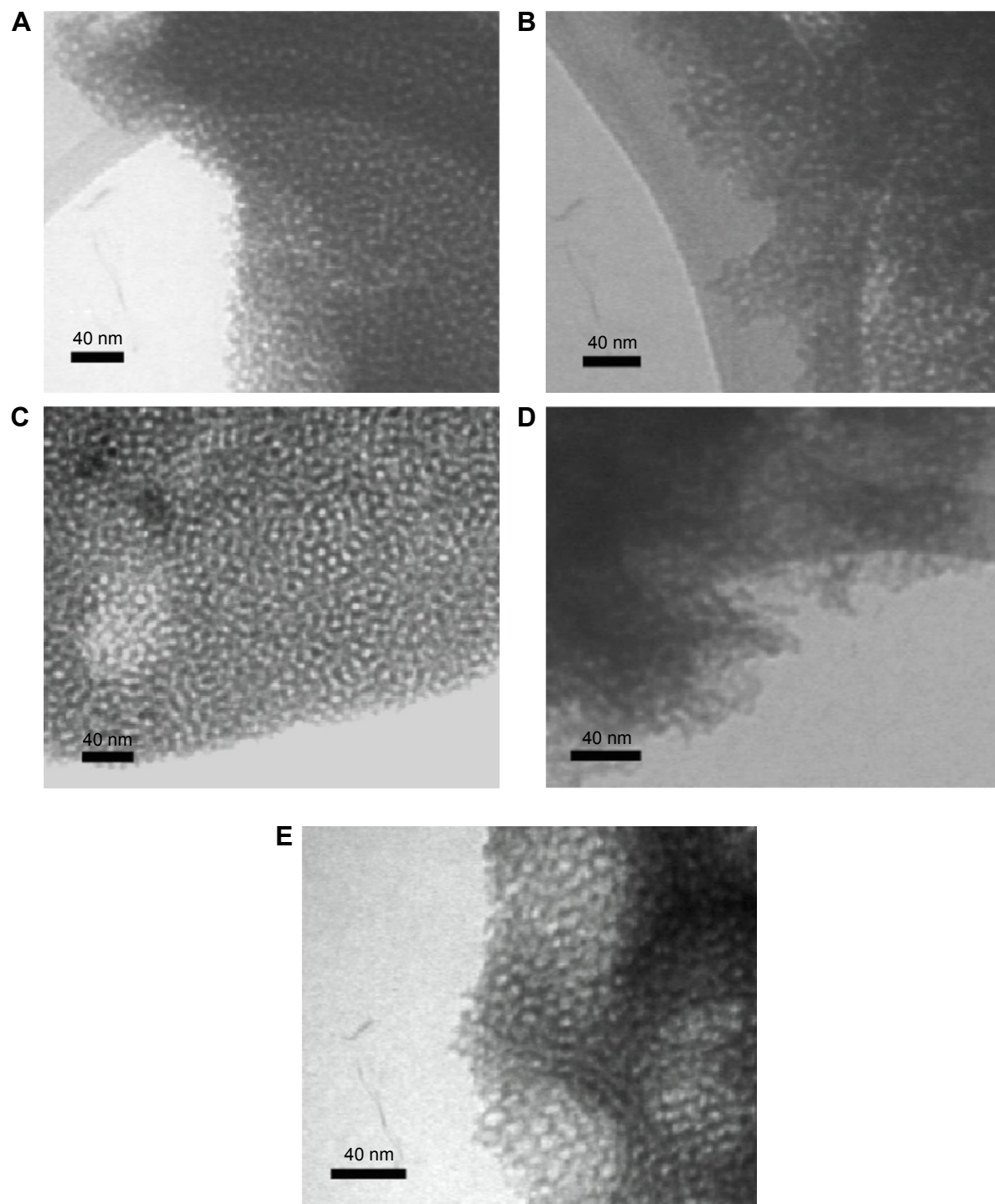


**Figure 2** TEM micrographs of the different prepared mesoporous titania films.

**Notes:** TEM micrographs of the different prepared mesoporous titania films using the following templates: **(A)** CTAB, **(B)** BRIJ S10, **(C)** P123, **(D)** P123:PPG with a ratio of 1:0.5 (PPG-0.5), and **(E)** P123:PPG with a ratio of 1:1 (PPG-1).

**Abbreviations:** CTAB, cetyltrimethylammonium bromide; PPG, poly(propylene glycol); TEM, transmission electron microscopy.

Surface functionalization using silane chemistry was used to alter the surface free energy of the mesoporous titania. Static CA measurements were carried out before and after surface functionalization, and the results are presented in Table 4. All the unmodified mesoporous surfaces were superhydrophilic

( $<5^\circ$ ), and the NP surface had a CA of  $8^\circ$ , which also is considered to be very hydrophilic. The surface functionalization by grafting dimethylsilane groups extensively increased the CA for all surfaces. This demonstrates that the free surface energy was lowered by the presence of dimethylsilane groups.

**Table 2** The average pore sizes measured in SEM and TEM images of the different samples

| Sample   | Average pore width (nm) |
|----------|-------------------------|
| CTAB     | 3.4                     |
| BRIJ S10 | 4.4                     |
| P123     | 6.0                     |
| PPG-0.5  | 6.5                     |
| PPG-I    | 7.2                     |

**Abbreviations:** SEM, scanning electron microscopy; TEM, transmission electron microscopy; CTAB, cetyltrimethylammonium bromide; PPG, poly(propylene glycol).

QCM-D experiments utilizing the density difference between H<sub>2</sub>O and D<sub>2</sub>O were conducted for all the different mesoporous coatings to examine the pore volume. In Table 5, the pore volume data are presented for the different samples, both with and without surface functionalization. The data demonstrated that the pore volume increased with larger pore sizes. Moreover, the presence of dimethylsilane groups slightly decreased the water-accessible pore volume capacity of the coatings.

### In vitro release kinetics

QCM-D was used to monitor the adsorption and desorption of ALN to examine the effect on kinetics when altering pore size and surface energy of the mesoporous titania thin films. A NP titania coating was used as reference to examine the difference with and without pores. Drug loading and release were monitored as shifts in frequency ( $\Delta f$ ). The obtained  $\Delta f$  was recalculated to mass ( $\Delta m$ ) using the Sauerbrey equation,

as shown in Equation 1, where  $C$  is the mass sensitivity constant (17.7 ng·Hz<sup>-1</sup>·cm<sup>-2</sup>) and  $n$  is the overtone number (1, 3, 5, etc).

$$\Delta m = -\frac{C \times \Delta f}{n} \quad (1)$$

The adsorption and release to/from the different surfaces in respect to the coating area, ie, the area exposed to the surroundings, are presented in Figure 5A and B. It was a general trend that the absorbed amount of ALN into the mesoporous films increased with a larger pore size. The adsorption of ALN to the NP titania was so small that it was merely detectable. This confirms that the majority of ALN is absorbed within the porous network of the mesoporous samples. Hence, a much higher drug loading is provided by the mesoporous structure. The adsorption monitoring was followed by addition of a rinsing flow of the pure solvent (Milli-Q H<sub>2</sub>O) to examine the release rate. An initial burst release of ALN was demonstrated for all the mesoporous surfaces; however, the release became sustained rather quickly. In the comparison between the unmodified and the hydrophobically modified surfaces, only minor differences in adsorption were observed. However, the release behavior differed between the unmodified and modified surfaces. The hydrophobized mesoporous surfaces had a higher degree of ALN released in the initial burst-release phase. The release behavior in the sustained delivery regime showed no major difference between the unmodified and modified surfaces.

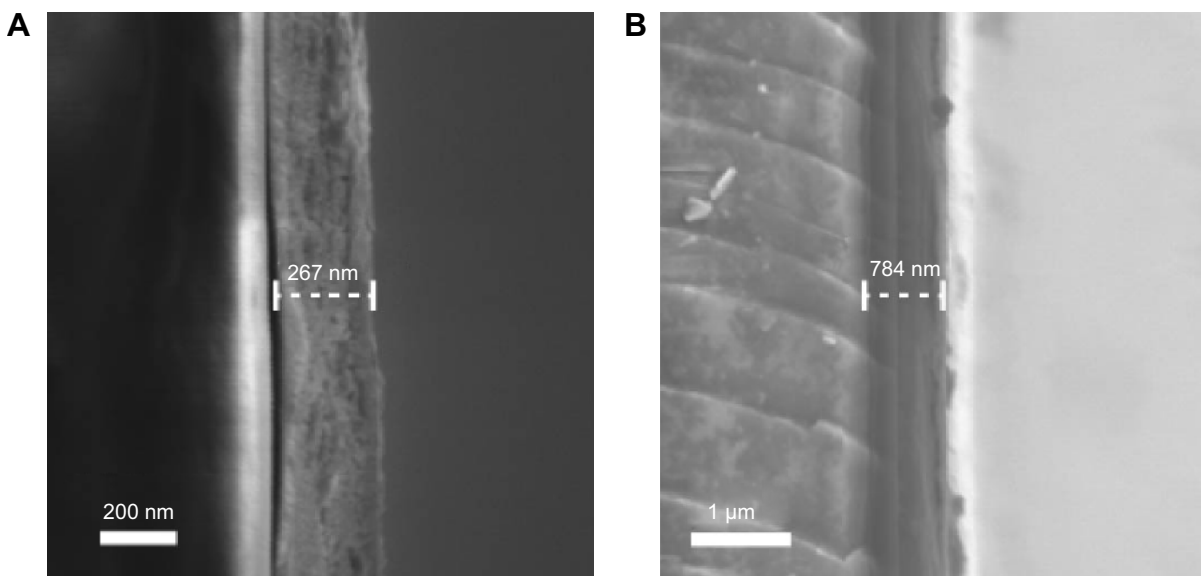


**Figure 3** SEM images of mesoporous titania film cross-sections coated on glass slides.  
**Notes:** Cross-sections of (A) a BRIJ S10 coating and (B) a PPG-0.5 coating are shown.  
**Abbreviations:** PPG, poly(propylene glycol); SEM, scanning electron microscopy.

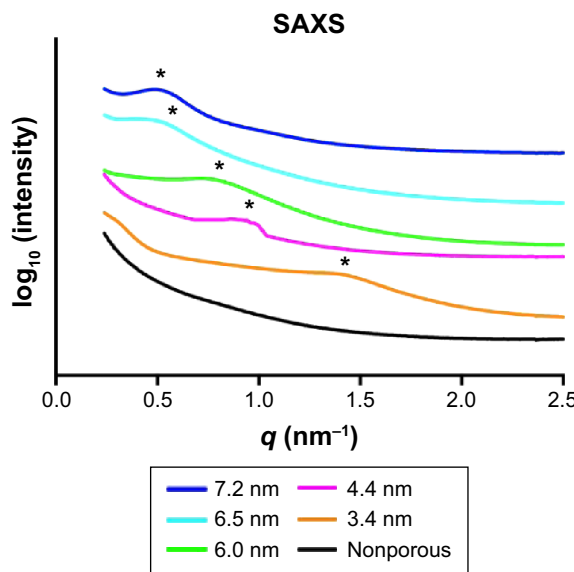


**Figure 4** SAXS data for the mesoporous titania films possessing different pore sizes and the nonporous titania.

**Notes:** The peak positions are marked with \*. The curves representing the different samples are separated in y-direction to simplify the visual comparison between them.

**Abbreviation:** SAXS, small angle X-ray scattering.

These data of adsorption and release to/from the coating area were also recalculated with respect to their internal area. The result of the accessible pore volume provides the relations of the internal area between the different mesoporous coatings. The recalculated data of adsorption and release in correlation to the internal area are presented in Figure 5C and D. Monitoring of the drug loading to the unmodified coatings demonstrate a general trend of higher drug adsorption per cm<sup>2</sup> of the internal surface area as a function of increased pore size. The hydrophobized surfaces showed no general trend, which suggest that the grafted methyl groups influence the adsorption.

It has previously been suggested that QCM-D is a suitable technique to determine molecular adsorption/desorption kinetics.<sup>41</sup> When a mesoporous material is used as drug host, the rate of the adsorption and desorption is affected by binding–diffusion kinetics. Hence, the adsorption and release kinetics can be described with the following equations:

**Table 3** XPS data presented as relative atomic% for the mesoporous titania thin films possessing different pore sizes

| Sample (nm) | Ti 2p (%) | O 1s (%) | C 1s (%) |
|-------------|-----------|----------|----------|
| 3.4         | 19.2      | 55.3     | 22.9     |
| 4.4         | 20.2      | 55.2     | 22.8     |
| 6.0         | 21.9      | 57.4     | 19.7     |
| 6.5         | 20.5      | 56.5     | 21.7     |
| 7.2         | 19.0      | 53.9     | 25.2     |

**Abbreviation:** XPS, X-ray photoelectron spectroscopy.

**Table 4** Contact angle for unmodified and surface-functionalized coatings

| Sample (nm) | Contact angle unmodified | Contact angle silane modified |
|-------------|--------------------------|-------------------------------|
| NP          | 8°                       | 100°                          |
| 3.4         | <5°                      | 85°                           |
| 4.4         | <5°                      | 85°                           |
| 6.0         | <5°                      | 80°                           |
| 6.5         | <5°                      | 107°                          |
| 7.2         | <5°                      | 110°                          |

**Notes:** The measurements were performed with Milli-Q H<sub>2</sub>O as liquid.

**Abbreviation:** NP, nonporous.

$$\frac{\partial u}{\partial t} = D_1 \nabla^2 u - k_a u + k_d b \quad (2)$$

$$\frac{\partial b}{\partial t} = D_2 \nabla^2 b + k_a u - k_d b, \quad (3)$$

where  $u$  denotes the concentration of unbound molecules and  $b$  the concentration of bound molecules.<sup>42</sup> Moreover,  $D_1$  and  $D_2$  are the diffusion coefficients, and  $k_a$  and  $k_d$  are the rate constants for adsorption and desorption, respectively. The different kinetic regimes that were obtained for the mesoporous materials are shown in Figure 6. In this figure, the data for the 7.2 nm sample is presented, since it possess the highest amount of adsorption sites among the samples tested, and the different regimes thus become more apparent. Both the adsorption and release kinetics involved two regimes, and the rate depends on whether the binding isotherm or the diffusion is dominant. In the initial adsorption regime, the adsorption isotherm is the rate-limiting step. The slope in this regime was thereby determined by the adsorption rate constant ( $k_a$ ). The calculated  $k_a$  values for the samples are presented in Table 6. A higher  $k_a$  was obtained as the pore size increased for the unmodified samples. No trend was observed for the functionalized surfaces; most of them showed about the same adsorption rate per area unit of the internal area.

**Table 5** Pore volume of the mesoporous titania thin films obtained from QCM-D experiments utilizing the density difference between H<sub>2</sub>O and D<sub>2</sub>O

| Sample (nm) | Pore volume (%) nonmodified | Pore volume (%) silane modified |
|-------------|-----------------------------|---------------------------------|
| 3.4         | 42                          | 37                              |
| 4.4         | 55                          | 49                              |
| 6.0         | 57                          | 55                              |
| 6.5         | 60                          | 57                              |
| 7.2         | 75                          | 71                              |

**Abbreviation:** QCM-D, quartz crystal microbalance with dissipation.

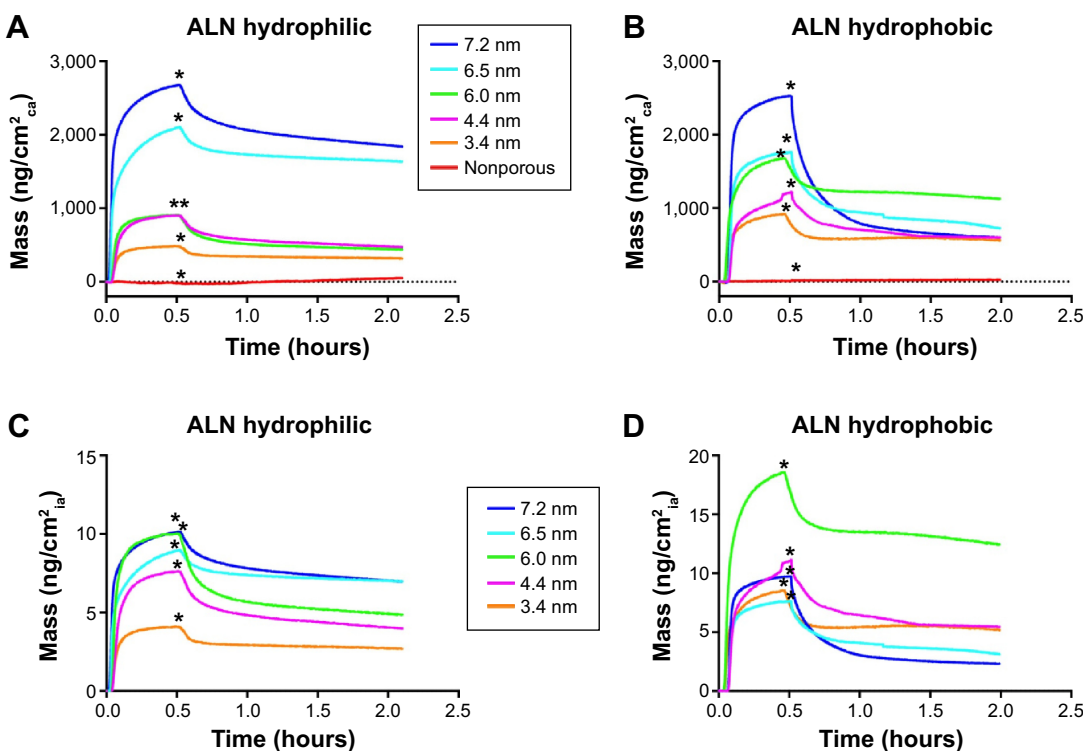


**Figure 5** QCM-D results of the adsorption and release of ALN.

**Notes:** The adsorption proceeded until the time point marked with \*; thereafter, the surfaces were rinsed with pure water to examine the release rate of ALN. The results are shown for both the unmodified mesoporous titania (**A**) and for the dimethylsilane treated materials (**B**) as the mass ALN per coating area (ca). In (**C**) and (**D**), the data are recalculated as mass per internal area (ia) for the unmodified and modified coatings, respectively.

**Abbreviations:** ALN, alendronate; QCM-D, quartz crystal microbalance with dissipation.

## Discussion

It was demonstrated from the SEM and TEM characterizations that the pore size of the mesoporous titania coatings could be tuned from 3.4 nm up to 7.2 nm by means of

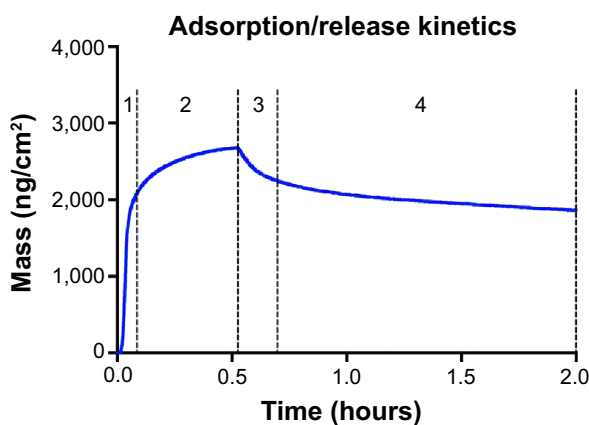


**Figure 6** QCM-D data for the 7.2 nm sample, displaying the different stages of ALN adsorption and release.

**Notes:** In (1), the adsorption kinetics is the rate-limiting factor. In (2), the rate-limiting factor of the adsorption is the diffusion factor. Between (2) and (3), the flow is changed to the rinsing flow, and the initial release (3) is determined by the molecular diffusion. The release becomes thereafter sustained (4) and the rate-limiting step is then the desorption isotherm.

**Abbreviations:** ALN, alendronate; QCM-D, quartz crystal microbalance with dissipation.

changing the structure-directing agents, CTAB, BRIJ S10, and P123, and by addition of PPG. This pore-size tunability provides the opportunity to host biologically active molecules ranging from small-molecular drugs up to macromolecules, such as proteins. It was also observed that the prepared coatings possessed a narrow pore-size distribution; this is a desirable property in order to reveal a reproducible and predictable release of the drugs. The pores were directed out from the surfaces, which is an essential requirement when using them as drug delivery systems. This is in contrast to preferential orientations for other applications, for example in photovoltaics where the desired pore direction is instead parallel to the surface.<sup>43</sup> Moreover, the results from the

**Table 6** The calculated adsorption rate constant,  $k_a$ , for both the unmodified and silane-modified samples in respect to their internal area (cm<sup>2</sup>)

| Sample (nm) | $k_a$ (ng·cm <sup>-2</sup> ·s <sup>-1</sup> )<br>unmodified | $k_a$ (ng·cm <sup>-2</sup> ·s <sup>-1</sup> )<br>silane-modified |
|-------------|---|--|
| 3.4         | 0.020   | 0.052  |
| 4.4         | 0.031   | 0.052  |
| 6.0         | 0.069   | 0.094  |
| 6.5         | 0.071   | 0.055  |
| 7.2         | 0.087   | 0.082  |

pore-size measurements using TEM and SEM correlated well with the obtained SAXS data, where the diffraction peaks were shifted toward lower  $q$ -values with increased pore size. However, the SAXS data showed only one peak in the pattern for the mesoporous titania thin films; hence, the pore symmetry could not be determined. The fact that the SEM images showed that the pores were directed out from the surface indicate that the mesoporous titania thin films possessed a bicontinuous structures. XPS showed that there was no significant chemical difference between the mesoporous titania thin films possessing different pore sizes. This result verifies that the pore size was tuned without changing the surface chemistry.

The addition of PPG as swelling agent did not only alter the pore sizes but also the film thickness, although the spin-coating parameters such as the rotational speed and the time were kept constant. The most probable reason for this is that a higher viscosity was noticed for the solutions that contained PPG, which subsequently resulted in thicker films during the spin-coating process. The coating thickness is an important property since it dictates the loading capacity of the mesoporous film. However, it is desirable to deposit relatively thin films onto the implants in order to preserve the screw geometry and to obtain a good biomechanical stability of the coating. The coating thickness never exceeded 800 nm for any of the formed films, which is favorable to avoid the risk of damaging the coating during implantation.

Besides tuning the pore size, the surface energy was also varied by grafting dimethylsilane groups onto the mesoporous titania, which resulted in highly reduced surface free energy. The choice of adding dimethylsilane groups after the formation of mesoporous titania is a preferable method over the one-pot synthesis since it provides higher density of functional groups.<sup>8</sup> The pore volume was examined to explore if it varied with changes in pore size and surface functionalization. As expected, it was demonstrated that an increased pore size also resulted in an increased pore volume. Notable is that the pore volume was considerably higher for the matrix with a pore size of 7.2 nm compared to all the other surfaces. Functionalization of the surfaces generally decreased the pore volume slightly compared to the native counterpart. This may due to the grafted molecules occupying some space, and the accessible pore volume thereby becoming lower. Another reason might be that the grafted hydrophobic species decreased the penetration of water inside the porous network to some extent.

The in vitro adsorption/release experiments demonstrated that both pore size and surface functionalization influenced the adsorption and acted as release modulators for the osteoporosis

drug ALN. The adsorption on the mesoporous surfaces was substantially higher compared to the NP, which was used as reference. Even though all the coatings were below 800 nm in thickness, which is desirable when using them as implant coatings, the porous structure provides considerably more adsorption sites. Moreover, a higher loading was observed as the pore size increased, which might be explained by more adsorption sites and a higher pore volume. The large difference observed for the surfaces prepared with swelling agent (6.5 nm and 7.2 nm samples) compared to the other samples could be explained by a considerably higher film thickness. In the comparison between the functionalized surface and its corresponding surface without modification, it was observed that a somewhat lower adsorption of drug was obtained for the functionalized surfaces. Probable reasons for this are that the functionalization molecules contribute to a decrease in pore size and that the penetration of the aqueous ALN solution was somewhat lower due to the hydrophobized pore walls.

Moreover, the adsorption data were recalculated in respect to the internal area of the different porous coatings. When comparing the unmodified samples, it was demonstrated that a higher adsorption per internal surface area as a function of pore size was obtained. This suggests that a larger pore size enables the drug molecules to adsorb as multilayers onto the pore walls. The lower pore sizes do not provide enough space for the drug molecules to adsorb as multilayers since the diameter of a drug molecule is approximately 1 nm, as shown in Figure 7. Hence, the adsorption follows the accessible pore volume, which increases as a function of pore size. This trend was not observed for the surface-functionalized coatings. The reason for this is probably that the methylated surface reduced the drug–surface interactions.

The adsorption monitoring was followed with a rinsing flow to examine the release rate. It showed that a higher amount of drug was liberated in the initial burst-release regime as the pore size was increased. This is in correlation to a higher adsorption per surface unit of internal surface area that was obtained as function of pore size. Hence, an increased multilayer buildup of the drug to the pore wall induces a higher degree of the initial burst release. This suggests stronger attachment of drug

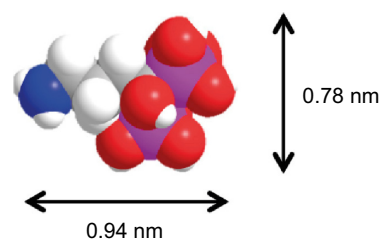


**Figure 7** The molecular structure and size of the osteoporosis drug alendronate (ALN).

molecules directly at the surface of the host material compared to the add-on layers in the multilayer arrangement. In the second regime, where the delivery becomes sustained, the release was slower as the pore size decreased. This is probably due to the binding isotherm having a larger effect compared to the diffusion for the samples with a lower pore size. It was also displayed that the hydrophobized surfaces had a larger degree of the initial burst release. This demonstrates that the functional groups reduced the affinity between the drug molecules and the pore walls. The hydrophobized surface with a pore size of 7.2 nm demonstrated the highest degree of initial release, which indicates highest degree of functionalization for this sample group. However, complete surface functionalization of the pore walls was probably not obtained since water penetration was still high.

The adsorption and release experiments were carried out using QCM-D that enables *in situ* monitoring. From the results, the adsorption kinetics can be divided into two regimes (Figure 6), where the adsorption isotherm is controlling the kinetics in the initial stage due to excessive amount of adsorption sites for the free drug molecules. As availability of adsorption sites decrease and more molecules become attached, the diffusion factor becomes more apparent. Since the initial regime of the adsorption was determined by the adsorption isotherm,  $k_a$  could be calculated. It was observed that  $k_a$  increased as a function of pore size for the unmodified samples in respect to their internal surface areas. This indicates increased multilayer adsorption of ALN as the accessible pore volume increased. There was no apparent trend between the surface-modified samples of different pore sizes. The reason for this is probably due to an increased efficiency of the surface functionalization with a higher pore size. Moreover, the release mechanism also consisted of two regimes, which is according to what has been observed when using mesoporous silica.<sup>44</sup> The initial release regime consists mainly of drug molecules that diffused rather freely, and as the release proceeded, it became mainly determined by the binding isotherm. In the later sustained-release regime, the drug molecules are highly influenced by the interactions of the pore walls, following a dynamic process of adsorbing and desorbing prior to being released out to the surrounding. This supports previous findings that the attractive van der Waals interactions between drug molecules and the pore walls play a significant role on the release profiles when using a mesoporous material.<sup>45</sup> The release behavior, with an initial release that is rather rapid followed by a sustained release profile, is most often a desired administration since the therapeutic level of the drug is obtained quickly and the sustained delivery ensures that the level is maintained.

## Conclusion

In this study, the pore size of mesoporous titania thin films was tuned from 3.4 nm up to 7.2 nm by the use of different structure-directing agents and with the addition of PPG as a swelling agent. Surface functionalization was performed using silane chemistry, which highly altered the surface energy of the mesoporous titania. *In situ* monitoring carried out using QCM-D allowed for examination of both the adsorption and release mechanisms when using a mesoporous thin film as drug host. The rate-limiting step in the different regimes of the adsorption and release is either determined by diffusion or by the binding isotherm. Moreover, it was demonstrated that the adsorption and release of the osteoporosis drug ALN were highly influenced both by the altered pore size and surface functionalization. Tuning these properties would provide an optimized temporal control of the release kinetics and loading capacity. In addition, by varying the pore size, the possibility of using mesoporous titania coatings as host for biologically active molecules ranging from small-molecular drugs up to proteins is feasible. This ability makes them an interesting drug delivery platform for improved functionalities of bone-anchoring implants.

## Acknowledgments

The financial support for this work was provided from the Materials Sciences Area of Advance at Chalmers University of Technology. We acknowledge the Maxlab synchrotron facility in Lund, Sweden, for giving us the opportunity and assistance to perform synchrotron SAXS measurements. We also thank Professor Anette Larsson and Professor Fredrik Höök at Chalmers University of Technology for their inputs to this work.

## Disclosure

The authors report no conflicts of interest in this work.

## References

1. Puleo DA, Nanci A. Understanding and controlling the bone-implant interface. *Biomaterials*. 1999;20(23–24):2311–2321.
2. Colilla M, Manzano M, Vallet-Regi M. Recent advances in ceramic implants as drug delivery systems for biomedical applications. *Int J Nanomedicine*. 2008;3(4):403–414.
3. Lin JH. Bisphosphonates: a review of their pharmacokinetic properties. *Bone*. 1996;18(2):75–85.
4. Kimmel DB. Mechanism of action, pharmacokinetic and pharmacodynamic profile, and clinical applications of nitrogen-containing bisphosphonates. *J Dent Res*. 2007;86(11):1022–1033.
5. Russell RG, Watts NB, Ebetino FH, Rogers MJ. Mechanisms of action of bisphosphonates: similarities and differences and their potential influence on clinical efficacy. *Osteoporos Int*. 2008;19(6):733–759.
6. Wermelin K, Suska F, Tengvall P, Thomsen P, Aspenberg P. Stainless steel screws coated with bisphosphonates gave stronger fixation and more surrounding bone. *Histomorphometry in rats*. *Bone*. 2008;42(2):365–371.
7. Abtahi J, Agholme F, Sandberg O, Aspenberg P. Effect of local vs systemic bisphosphonate delivery on dental implant fixation in a model of osteonecrosis of the jaw. *J Dent Res*. 2013;92(3):279–283.

8. Song SW, Hidajat K, Kawi S. Functionalized SBA-15 materials as carriers for controlled drug delivery: influence of surface properties on matrix-drug interactions. *Langmuir*. 2005;21(21):9568–9575.
9. Yang P, Quan Z, Li C, Kang X, Lian H, Lin J. Bioactive, luminescent and mesoporous europium-doped hydroxyapatite as a drug carrier. *Biomaterials*. 2008;29(32):4341–4347.
10. Wang S. Ordered mesoporous materials for drug delivery. *Microporous Mesoporous Mater*. 2009;117(1–2):1–9.
11. Zhu M, Zhu Y, Ni B, et al. Mesoporous silica nanoparticles/hydroxyapatite composite coated implants to locally inhibit osteoclastic activity. *ACS Appl Mater Interfaces*. 2014;6(8):5456–5466.
12. Vallet-Regi M, Balas F, Arcos D. Mesoporous materials for drug delivery. *Angew Chem Int Ed Engl*. 2007;46(40):7548–7558.
13. Izquierdo-Barba I, Colilla M, Vallet-Regi M. Nanostructured mesoporous silicas for bone tissue regeneration. *J Nanomater*. 2008;2008:106970.
14. Xu M, Feng D, Dai R, Wu H, Zhao D, Zheng G. Synthesis of hierarchically nanoporous silica films for controlled drug loading and release. *Nanoscale*. 2011;3(8):3329–3333.
15. Crepaldi EL, Soler-Illia G, Gross D, Cagnol F, Ribot F, Sanchez C. Controlled formation of highly organized mesoporous titania thin films: from mesostructured hybrids to mesoporous nanoanatase  $TiO_2$ . *J Am Chem Soc*. 2003;125(32):9770–9786.
16. Brinker CJ, Lu YF, Sellinger A, Fan HY. Evaporation-induced self-assembly: nanostructures made easy. *Adv Mater*. 1999;11(7):579–585.
17. Gross D, Cagnol F, Soler-Illia G, et al. Fundamentals of mesostructuring through evaporation-induced self-assembly. *Adv Funct Mater*. 2004;14(4):309–322.
18. Soler-Illia GJ, Angelome PC, Fuertes MC, Gross D, Boissiere C. Critical aspects in the production of periodically ordered mesoporous titania thin films. *Nanoscale*. 2012;4(8):2549–2566.
19. McMaster WA, Wang X, Caruso RA. Collagen-templated bioactive titanium dioxide porous networks for drug delivery. *ACS Appl Mater Interfaces*. 2012;4(9):4717–4725.
20. Xia W, Grandfield K, Hoess A, Ballo A, Cai Y, Engqvist H. Mesoporous titanium dioxide coating for metallic implants. *J Biomed Mater Res B Appl Biomater*. 2012;100(1):82–93.
21. Mendes VC, Moineddin R, Davies JE. The effect of discrete calcium phosphate nanocrystals on bone-bonding to titanium surfaces. *Biomaterials*. 2007;28(32):4748–4755.
22. Joos U, Wiesmann HP, Szuwart T, Meyer U. Mineralization at the interface of implants. *Int J Oral Maxillofac Surg*. 2006;35(9):783–790.
23. Yan W-Q, Nakamura T, Kobayashi M, Kim H-M, Miyaji F, Kokubo T. Bonding of chemically treated titanium implants to bone. *J Biomed Mater Res*. 1997;37(2):267–275.
24. Grandfield K, Gustafsson S, Palmquist A. Where bone meets implant: the characterization of nano-osseointegration. *Nanoscale*. 2013;5(10):4302–4308.
25. Karlsson J, Sundell G, Thuvander M, Andersson M. Atomically resolved tissue integration. *Nano Lett*. 2014;14(8):4220–4223.
26. Karlsson J, Jimbo R, Fathali HM, et al. In vivo biomechanical stability of osseointegrating mesoporous  $TiO_2$  implants. *Acta Biomater*. 2012;8(12):4438–4446.
27. Harmankaya N, Karlsson J, Palmquist A, et al. Raloxifene and alendronate containing thin mesoporous titanium oxide films improve implant fixation to bone. *Acta Biomater*. 2013;9(6):7064–7073.
28. Galli S, Naito Y, Karlsson J, et al. Osteoconductive potential of mesoporous titania implant surfaces loaded with magnesium: an experimental study in the rabbit. *Clin Implant Dent Relat Res*. Epub February 20, 2014.
29. Galli S, Naito Y, Karlsson J, et al. Local release of magnesium from mesoporous  $TiO_2$  coatings stimulates the peri-implant expression of osteogenic markers and improves osteoconductivity in vivo. *Acta Biomater*. 2014;10(12):5193–5201.
30. Karlsson J, Harmankaya N, Allard S, et al. Ex vivo alendronate localization at the mesoporous titania implant/bone interface. *J Mater Sci Mater Med*. 2015;26(1):1–8.
31. Höök F, Vörös J, Rodahl M, et al. A comparative study of protein adsorption on titanium oxide surfaces using in situ ellipsometry, optical waveguide lightmode spectroscopy, and quartz crystal microbalance/dissipation. *Colloids Surf B Biointerfaces*. 2002;24(2):155–170.
32. Coquil T, Richman EK, Hutchinson NJ, Tolbert SH, Pilon L. Thermal conductivity of cubic and hexagonal mesoporous silica thin films. *J Appl Phys*. 2009;106(3):034910–034911.
33. Besson S, Gacoin T, Ricolleau C, Jacquiod C, Boilot J-P. Phase diagram for mesoporous CTAB-silica films prepared under dynamic conditions. *J Mater Chem*. 2003;13(2):404–409.
34. Alberius PCA, Frindell KL, Hayward RC, Kramer EJ, Stucky GD, Chmelka BF. General predictive syntheses of cubic, hexagonal, and lamellar silica and titania mesostructured thin films. *Chem Mater*. 2002;14(8):3284–3294.
35. Andersson M, Birkedal H, Franklin NR, et al. Ag/AgCl-loaded ordered mesoporous anatase for photocatalysis. *Chem Mater*. 2005;17(6):1409–1415.
36. Wu QL, Rankin SE. Tuning the mesopore size of titania thin films using a polymeric swelling agent. *J Phys Chem C*. 2011;115(24):11925–11933.
37. Wu QL, Subramanian N, Rankin SE. Hierarchically porous titania thin film prepared by controlled phase separation and surfactant templating. *Langmuir*. 2011;27(15):9557–9566.
38. Andreatta GI, Jian Wang Y, Kay Lee F, et al. Molecular transfer of surfactant bilayers: widening the range of substrates. *Langmuir*. 2008;24(12):6072–6078.
39. Almanza-Workman AM, Raghavan S, Petrovic S, et al. Characterization of highly hydrophobic coatings deposited onto pre-oxidized silicon from water dispersible organosilanes. *Thin Solid Films*. 2003;423(1):77–87.
40. Sauerbrey G. Verwendung von Schwingquarzen zur Wägung dünner Schichten und zur Mikrowägung [Use of quartz crystal methods to determine the weight of adsorbed layers with high sensitivity]. *Zeitschrift für Physik A Hadrons and Nuclei*. 1959;155(2):206–222. German.
41. Wu B, Wu K, Wang P, Zhu D-M. Adsorption kinetics and adsorption isotherm of poly(N-isopropylacrylamide) on gold surfaces studied using QCM-D. *J Phys Chem C*. 2007;111(3):1131–1135.
42. Schuster E, Hermansson A-M, Ohgren C, Rudemo M, Loren N. Interactions and diffusion in fine-stranded  $\beta$ -lactoglobulin gels determined via FRAP and binding. *Biophys J*. 2014;106(1):253–262.
43. Ivanova A, Fattakhova-Rohlfing D, Kayaalp BE, Rathouský J, Bein T. Tailoring the morphology of mesoporous titania thin films through biotemplating with nanocrystalline cellulose. *J Am Chem Soc*. 2014;136(16):5930–5937.
44. Lian H-Y, Liang Y-H, Yamauchi Y, Wu KCW. A hierarchical study on load/release kinetics of guest molecules into/from mesoporous silica thin films. *J Phys Chem C*. 2011;115(14):6581–6590.
45. Ukmar T, Maver U, Planinšek O, Kaučič V, Gaberšček M, Godec A. Understanding controlled drug release from mesoporous silicates: theory and experiment. *J Control Release*. 2011;155(3):409–417.